Original article

Nuclear Medicine Communications

A phantom assessment of portable imaging and radio-guided surgery systems with technetium-99m and fluorine-18

Thomas Krohn, Frederik A. Verburg, Holger Brockmann, Oliver H. Winz, Felix M. Mottaghy and Florian F. Behrendt

Aim **To perform a detailed analysis of the performance of mobile intraoperative imaging systems and gamma probes in a phantom set-up, and compare this with a conventional gamma camera.**

Methods **Two separate experiments were performed. In the first, a modified Jaszczak phantom equipped with five ^{99m}Tc-filled hot spheres (0.5–20 ml) was analyzed using Sentinella, declipseSPECT and a conventional gamma camera under three conditions: no background, spheres on the surface of the background activity, and totally immersed spheres (contrast level in both 1:8). In the second experiment, two phantom spheres (0.5 and 2 ml) filled with ^{99m}Tc and ^{18}F (infinite contrast, 1:4 and 1:8) were measured using the hand-held probes Navigator and GammaLocator DXI. Data analysis consisted of signal-to-background ratios and determination of the full-width at half-maximum (FWHM). A visual scoring was performed by three nuclear medicine physicians.**

Results **At infinite contrast, ^{99m}Tc-filled spheres with volumes of at least 2 ml could be detected adequately with all systems (e.g. 2 ml sphere, FWHM: ECAM 11 mm, declipseSPECT 9 mm, Navigator 13 mm, GammaLocator 12 mm). Under decreased contrast conditions, the results for all systems were impaired and the 0.5 ml phantom sphere filled with either ^{99m}Tc or ^{18}F was only detected accurately by the GammaLocator (FWHM range: 13–17 mm).**

Conclusion **All systems are suitable for intraoperative sentinel node detection with nearly infinite signal-to-background contrast. At a lower contrast, the GammaLocator performed best for the detection of small volumes at low-contrast ratios regardless of the radionuclide. *Nucl Med Commun* 33:452–458 © 2012 Wolters Kluwer Health | Lippincott Williams & Wilkins.**

Nuclear Medicine Communications 2012, **33**:452–458

Keywords: gamma probe, intraoperative imaging, intraoperative positron emission tomography, scintigraphy

Department of Nuclear Medicine, University Hospital Aachen, RWTH Aachen University, Aachen, Germany

Correspondence to Thomas Krohn, MD, Department of Nuclear Medicine, University Hospital Aachen, Pauwelsstrasse 30, 52074 Aachen, Germany
Tel: +49 241 808 8743; fax: +49 241 808 2520; e-mail: tkrohn@ukaachen.de

Received 23 August 2011 **Revised** 24 November 2011
Accepted 17 December 2011

Introduction

Specific radiotracers are used for preoperative staging and radio-guided surgery of various malignancies in daily nuclear medicine routines all over the world [1–4]. Hand-held gamma probes provide an accurate and simple method for intraoperative localization of small lesions with radiotracer uptake, which would be difficult to find otherwise. A widely established typical example of such procedures using a ^{99m}Tc-labeled tracer is the sentinel lymph node biopsy (SLNB) [5–7]. Because the SLNB is mostly characterized by high signal-to-background ratios, the lesion localization often is technically easy. The presence of a 'hot' injection site can, however, be a huge challenge when searching for a small sentinel lymph node containing a low activity concentration, as the signal-to-background ratio in this case can be considerably lower [8]. In addition, in other potential applications of radio-guided surgery, such as localization of ^{99m}Tc-MIBI-positive parathyroid tumors, intraabdominal lymph nodes or octreotide-positive lesions [5,9], much lower signal-to-background ratios have to be expected. This in turn requires a higher technical performance from measurement equipment in order to accurately localize a lesion of interest.

In addition to the conventional gamma emitter-labeled radiotracers, radio-guided surgery with specific PET tracers like ^{18}F-choline, ^{18}F-DOPA, or ^{68}Ga-DOTATOC is desirable [10,11]. The use of these tracers in radio-guided surgery would allow for the detection and removal of small tumor lesions whose intraoperative localization might be difficult otherwise [12]. However, in contrast to low-energy conventional gamma imaging tracers (^{99m}Tc: 141 keV), precise collimation of 511 keV radiation emitted by PET tracers poses a considerable technical challenge.

For conventional gamma probe measurements, a variety of equipment with different designs is available [13]. Supplementary to conventional gamma probes, innovative solutions for intraoperative radiation measurement and imaging have been developed recently such as an electronically collimated 511 keV gamma probe and two new systems that allow for intraoperative nuclear imaging with low-energy radiotracers. Although these systems appear promising, a detailed analysis of their performance and a comparison with conventional systems are still lacking. Therefore, the aim of this study was to compare

0143-3636 © 2012 Wolters Kluwer Health | Lippincott Williams & Wilkins

DOI: 10.1097/MNM.0b013e3283508577

the performance of these new systems for intraoperative imaging under standardized conditions using a phantom model, using conventional planar scintigraphy as a reference standard.

Materials and methods

Clinical basis

To investigate clinically realistic activity concentrations and contrast ratios within small tumors, we analyzed planar scintigrams from five SLNBs and five parathyroid adenomas (PA) using a region-of-interest-based technique (MultiModality imaging tool; Hermes Medical, Stockholm, Sweden). Scintigrams were acquired using a conventional gamma camera with a large field of view (ECAM; Siemens, Erlangen, Germany) 3 h after injection of 70 ± 15 MBq ^{99m}Tc-nanoparticles for SLNB or 2 h after injection of 400 ± 50 MBq ^{99m}Tc-MIBI for PA. The acquisition time was 5 min per image. An activity concentration of about 10 kBq/ml was found to be a realistic value for small lesions. For the SLNB, an average contrast ratio (lesion to background) of 120.3 ± 58.1 (mean ± SD) was found in the scintigrams. This represents the lower end estimate of the realistic clinical situation as we used a ^{57}Co flood source to simultaneously image the body outline, thus falsely elevating the background activity. For PA, the contrast ratio was much lower at 1.9 ± 0.7.

Gamma cameras for intraoperative use

Recently, two portable camera systems for intraoperative use have been introduced: Sentinella (OncoVision, Valencia, Spain) and the freehand single-photon emission computed tomography (SPECT) system declipseSPECT (surgicEye, Munich, Germany).

Sentinella is a portable planar gamma camera system using a CsI(Na) scintillation crystal with a field of view of 40 × 40 mm, which can be used in an energy range of 50–200 keV. Two pinhole and a diverging collimator are available; in our study, the pinhole collimator with a hole diameter of 4 mm was used. Images can be displayed in real time on a persistence scope as well as in the form of planar scintigrams.

Freehand SPECT consists of a hand-held gamma probe fitted with a three-dimensional (3D) optical tracking system. The patient is monitored by an optical camera; probe and patient position are continuously monitored by two additional infrared cameras through sphere markers. Image acquisition is performed by scanning the volume of interest with the gamma probe from several different positions and angles, after which a 3D image reconstruction algorithm is started. The resulting scintigram is displayed as a fusion on top of the optical patient image. The system is mainly suitable for imaging with ^{99m}Tc/141 keV radiopharmaceuticals; acquisition at higher energy levels (i.e. ^{131}I/364 keV) is currently under investigation.

For the appraisal of the portable camera and freehand SPECT probes for imaging in the range of conventional radionuclides, a modified Jaszczak phantom consisting of six hollow spheres with volumes of 0.5, 1, 2, 5.5, 11, and 20 ml fixed inside a 6.6 l acrylic cylinder was used. Spheres were filled with 10 kBq/ml ^{99m}Tc. Acquisitions were performed with an empty glass cylinder for infinite contrast and with a signal-to-background ratio of 1 : 8 (background activity: 1.25 kBq/ml ^{99m}Tc) under two different conditions: first, with the phantom cylinder filled up to the equator of the spheres, so that the spheres were on the surface of the background activity; and second, with the cylinder completely filled so that the spheres were completely immersed in the background activity. The acquisition time was 3 min for each condition for each device.

Gamma probes

Two commercially available gamma probes have been examined in this study: RMD Navigator (RMD Instruments Corp., Watertown, Massachusetts, USA) and GammaLocator DXI (GF&E-Tec, Seeheim, Germany).

The Navigator is a conventional gamma probe with mechanical collimation mainly designed for intraoperative SLNB with ^{99m}Tc and other low-energy radiopharmaceuticals. For this system, a high-energy probe designed for use with energies up to 511 keV that uses a large tungsten collimator is also available.

In contrast, the GammaLocator has no mechanical collimation. Instead, the probe consists of five semiconductor radiation detectors; signals are processed using a software algorithm that provides an electronic collimation by determining the direction of the radiation by differences in detection intensity by the different detectors. This system allows for radiation detection in a wide energy range from 120 keV up to 511 keV, so that all relevant radiopharmaceuticals are covered by one single probe system.

For examining the conventional probe and the electronically collimated probe, probes were installed on a stand. Measurements were performed using the 0.5 and 2 ml ^{99m}Tc-filled (10 kBq/ml) phantom spheres of the above-described modified Jaszczak phantom at infinite contrast and at signal-to-background ratios of 1:4 and 1:8 with spheres on the surface of the background activity and with completely immersed spheres. Count rates were measured on the center of each sphere and were averaged over 10 s. Then the phantom was shifted away from the probe incrementally in steps of 4 mm up to a maximum distance of 32 mm from the center of the sphere. Count rates were recorded again over 10 s for each step. This protocol was repeated with ^{18}F (10 kBq/ml in the spheres) instead of ^{99m}Tc.

For all conditions, the signal-to-background ratio was calculated as the quotient of the maximum count rate of

the phantom sphere and the count rate of the background activity.

Reference method

As a reference standard, all ^{99m}Tc phantom set-ups were acquired as planar images over 3 min on the aforementioned conventional gamma camera equipped with standard low-energy high-resolution collimators.

Image analysis

For each phantom sphere image, line profiles were generated using the open-source software tool AMIDE [14]. The resulting data sets (position and corresponding count rate) were fitted using the curve-fitting toolbox from MATLAB 2009b (The MathWorks inc., Natick, Montana, USA). All fits were based on a Gaussian model: $f(x)=a\times e^{[-(x-b)^2/2\times c^2]}$. The full-width at half-maximum (FWHM) of each curve was calculated using the formula: $FWHM = 2\times[(2\times\ln 2)^{1/2}]\times c$, where c is obtained from the first equation. The FWHM value represents the spatial resolution of the equipment.

In addition, a score-based visual analysis was performed by three experienced nuclear medicine physicians. The quality of each sphere image was graded using a five-point scale from 1 (very poor image quality) to 5 (excellent image). Table 1 summarizes the grading criteria. The mean score values were calculated from the three observers. Subsequently, summed scores were generated by adding the mean scores for each sphere and system under each condition.

Results

Gamma cameras

Qualitative analysis

Visual quality scoring showed that the conventional camera was deemed to have the best image quality of all measurements (Fig. 1a), except for smaller phantom spheres (volume 11 ml and less) on the surface of the background activity with a contrast level of 1:8 (Table 2). Under this condition, freehand SPECT scored slightly better (Fig. 1b).

For the contrast condition 1:8 with totally immersed spheres, spheres of 5.5 ml and smaller cannot be detected adequately by any of the systems. As imaging of the totally immersed phantom spheres with freehand SPECT yielded an implausible result; the data acquisition for this condition was repeated twice, with extremely poor reproducibility of the image and spheres could not be adequately identified (Fig. 1c).

Table 1 Grading scheme for image quality of the spheres

1	Very poor	Obscured image; sphere not detectable
2	Poor	Sphere rudimentary detectable
3	Fair	Sphere in total detectable, but borders of the sphere are inadequate for evaluation
4	Good	Sphere and its border are present at a level that allows proper but not excellent evaluation of the image
5	Excellent	Distinct detail of the sphere leading to clear and easy evaluation

Under all examined conditions, comparison of freehand SPECT with the portable camera showed better visual scores for freehand SPECT. The portable camera scored the worst of the three systems, with rapidly decreasing image quality once contrast is introduced. Contrary to the freehand SPECT and conventional camera, the smallest phantom spheres could not (0.5 ml) or could hardly (1.0 ml) be detected by the portable camera even under infinite contrast.

Quantitative analysis

Automatic calculation of FWHM values was performed by generating a line profile with AMIDE with subsequent Gaussian curve fitting by MATLAB (Fig. 2). The results of the detailed quantitative analysis are given in Table 3. At infinite contrast, the results for the conventional camera and freehand SPECT were very similar. For the contrast level of 1:8 with spheres on the surface of the background activity, freehand SPECT revealed much better results in comparison with the conventional camera. Nevertheless, under this condition, the smallest phantom sphere could be evaluated neither by the conventional camera nor by freehand SPECT (Fig. 3).

Imaging of the totally immersed phantom spheres at a contrast level of 1:8 with declipseSPECT showed a poor reproducibility. Although we were able to calculate FWHM values in despite this, they must be considered as having limited accuracy. For the Portable camera, FWHM values could not be calculated because this system is not calibrated for longitude measurement units.

Gamma probes

Conventional probe

At infinite contrast using ^{99m}Tc, the FWHM was 16 mm for the 2.0 ml phantom sphere and 13 mm for the 0.5 ml sphere.

With the spheres on the surface of the background activity, the count rate over the activity maximum in the 2.0 ml sphere was 2.1 times higher than the background activity (FWHM 18 mm) for a contrast ratio of 1:8 and 1.3 times higher at a contrast ratio of 1:4 (FWHM 22 mm). For the 0.5 ml sphere on the surface of the background activity, the signal-to-background ratio measured by the conventional probe was markedly impaired for both the 1:8 and the 1:4 contrast ratio: the count rate hardly decreased with increasing distance from the sphere (Fig. 4). Even directly over the sphere, the count rate was only 1.1 times higher than the background activity. Under these conditions, therefore, the FWHM could not be determined reliably.

With completely immersed spheres, the 2.0 ml sphere could be discriminated against the background activity at

Fig. 1

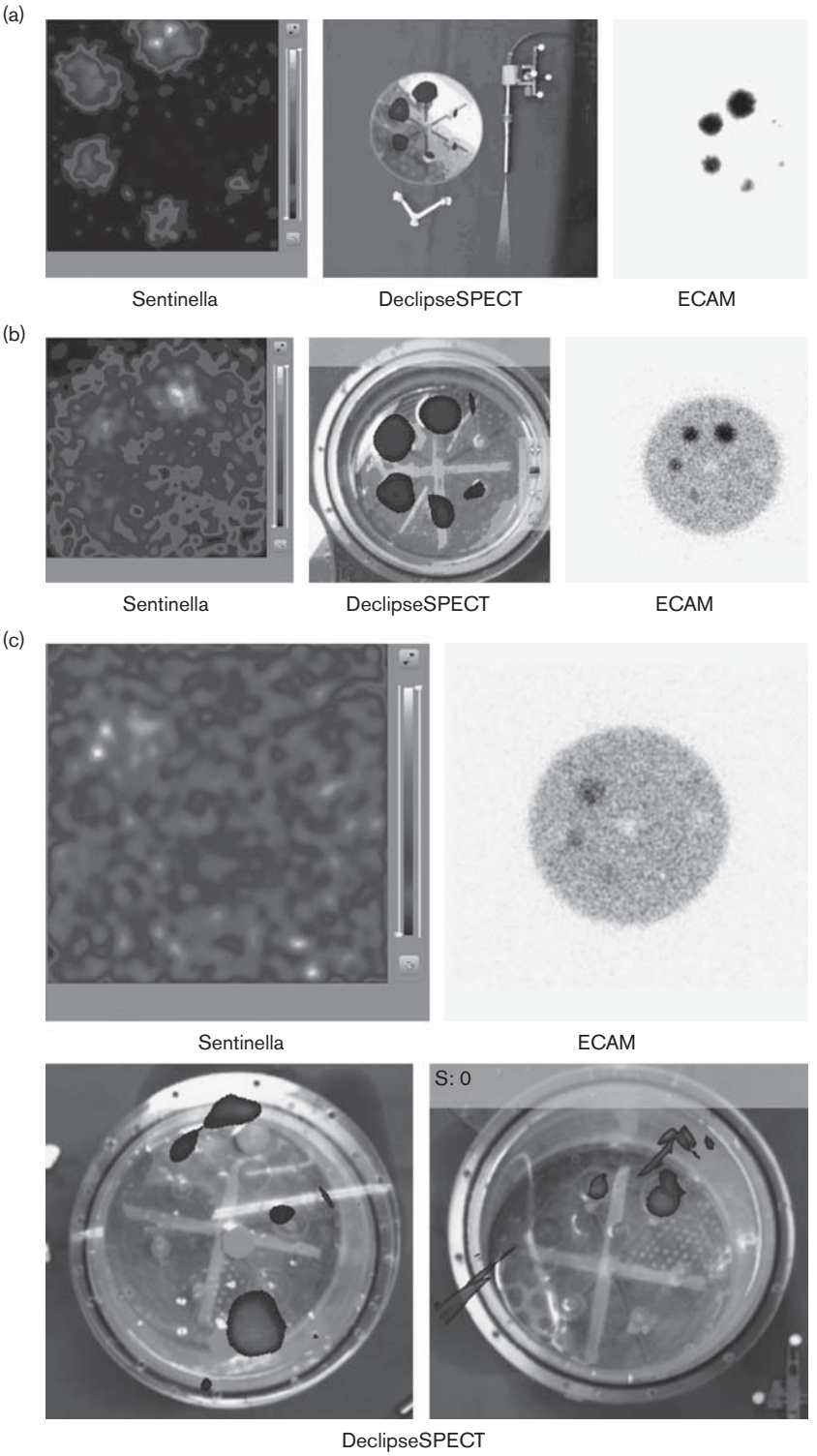

Comparison of scintigraphic images of the portable camera, freehand single-photon emission computed tomography (SPECT), and a conventional gamma camera. (a) Infinite contrast. (b) Contrast level of 1 : 8, spheres on surface of the background activity. (c) Comparison of scintigraphic images of the portable camera and the conventional camera at a contrast level of 1 : 8 with totally immersed spheres; the two images of the freehand SPECT show that reproducibility may be poor under this condition.

Table 2 Average qualitative scores of the sphere images from the three observers

Condition	Sphere volume (ml)	ECAM ^{99m}Tc	DeclipseSPECT ^{99m}Tc	Sentinella ^{99m}Tc
Infinite contrast	20	5.0	4.7	4.0
	11	5.0	4.7	3.3
	5.5	4.3	4.7	3.0
	2	4.3	3.7	2.0
	1	4.0	3.3	1.3
	0.5	3.3	2.7	1.0
	Sum	26.0	23.7	14.7
Contrast 1:8 with spheres on surface	20	4.7	4.0	3.0
	11	4.0	4.7	2.0
	5.5	3.7	4.3	1.3
	2	2.3	3.0	1.0
	1	1.0	2.0	1.0
	0.5	1.0	2.0	1.0
	Sum	16.7	20.0	9.3
Contrast 1:8 with totally immersed spheres	20	4.0	3.3	2.0
	11	3.0	2.7	1.0
	5.5	2.0	1.0	1.0
	2	1.0	1.0	1.0
	1	1.0	1.0	1.0
	0.5	1.0	1.0	1.0
	Sum	12.0	10.0	7.0

Table 3 Quantitative analysis: full-width at half-maximum in (mm)

Condition	Sphere volume (ml)	ECAM ^{99m}Tc	DeclipseSPECT ^{99m}Tc
Infinite contrast	20	25.2	22.5
	11	19.6	26.2
	5.5	16	21.6
	2	11.3	8.5
	1	9.2	6.9
	0.5	8.6	NA
Contrast 1:8 with spheres on surface	20	44.2	22.5
	11	64.1	29.1
	5.5	NA	19.9
	2	NA	13.1
	1	NA	13.1
	0.5	NA	NA
Contrast 1:8 with totally immersed spheres	20	NA	(23.1)[a]
	11	NA	(18.3)[a]
	5.5	NA	NA

For the portable camera, full-width at half-maximum values could not be calculated because this system is not calibrated for longitude measurement units. NA, automatic curve fitting was not possible due to image noise even when spheres were visually discernable.
[a]For these results, reproducibility was very poor for subsequent image acquisitions.

Fig. 2

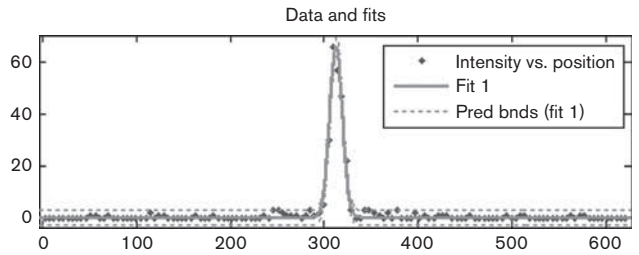

Measurement of full-width at half-maximum by curve fitting with MATLAB. Example of an ideal condition: conventional camera with a phantom volume of 5.5 ml at infinite contrast. Pred bnds, 95% confidence prediction bounds.

Fig. 3

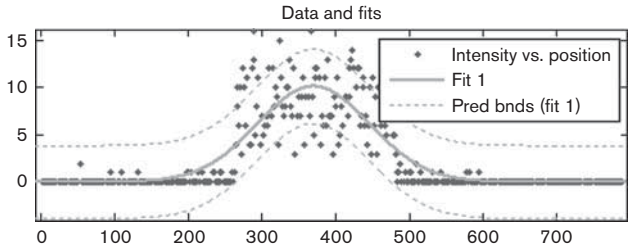

Example: conventional camera with a totally immersed 5.5 ml sphere at a contrast level of 1:8. Automatic calculation of full-width at half-maximum was not possible due to low image contrast. Pred bnds, 95% confidence prediction bounds.

a contrast level of 1:8 (FWHM 25 mm). At a contrast level of 1:4, the 2.0 ml sphere could not be detected. The 0.5 ml sphere could not be detected at either contrast ratio under this condition.

When using the conventional probe with the high-energy probe for ^{18}F, the 0.5 and the 2.0 ml spheres could be detected at infinite contrast with an FWHM of 28 and 32 mm, respectively.

With spheres on the surface and a contrast level of 1:8, only the 2.0 ml sphere could be discriminated against the background activity. The measured signal-to-background ratio was 1.3 at an FWHM of 37 mm. At a contrast level of 1:4, the 2.0 ml sphere was not detectable. The 0.5 ml sphere was not detectable at either contrast level.

With totally immersed spheres, neither the 2.0 ml nor the 0.5 ml sphere could be discriminated against the background activity even at a contrast level of 1:8.

Electronically collimated probe

At infinite contrast, the ^{99m}Tc-filled 0.5 and 2.0 ml sphere could be detected with an FWHM of 11 and 12 mm, respectively. Because the probe was calibrated using the background activity as zero, a signal-to-background ratio could not be calculated. The 0.5 and 2.0 ml spheres on the surface of the background activity showed comparable results for contrast ratios of 1:8 or 1:4 with an FWHM in the range of 15–17 mm. For totally immersed spheres, the FWHM values for both spheres at both contrast ratios were in the range of 13–16 mm.

When using ^{18}F, both phantom spheres were detectable with an FWHM of 24–25 mm at infinite contrast as well

Fig. 4

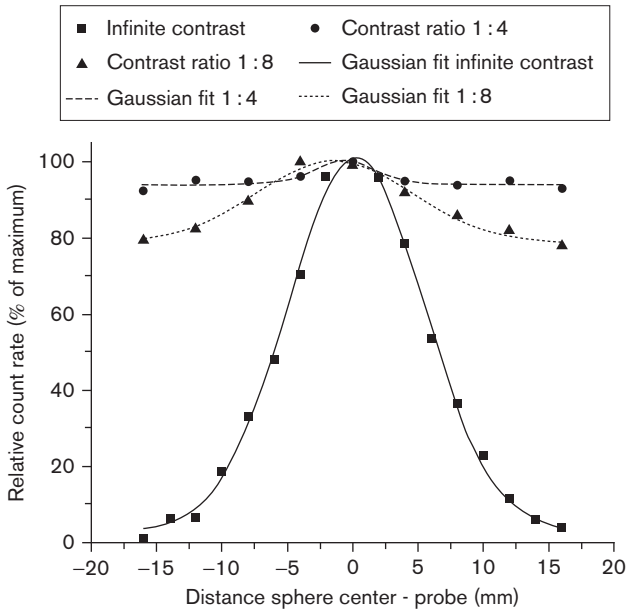

Count rates of the conventional probe for the 0.5 ml phantom sphere on the surface of the background activity.

as when spheres were on the surface of the background activity at both contrast levels (1: 8 and 1: 4). FWHM of totally immersed spheres was in the range of 21–24 mm for both spheres and contrast conditions.

Discussion

With an ever-increasing number of specific radiotracers available for use in clinical routine, intraoperative detection and visualization of small lesions with radiotracer uptake is becoming increasingly important [12,15]. Radio-guided surgery may provide an important tool for detection of small lesions that would have otherwise been overlooked, preventing curative treatment. A multitude of devices for use in such procedures is available on the market. In the present study, four of these have been assessed: two gamma probes and two mobile gamma-camera systems.

Although the clinical use of most of these systems has been reported before in separate papers [5,6,10,16], as far as we could ascertain, no similar comparison of mobile devices for γ-ray detection and imaging has been reported before in the literature.

A potential limitation of the present study is that the comparison of the different systems was performed using only a phantom model and not under real surgical conditions, thereby potentially underestimating practical issues in the use of the devices. However, a phantom set-up provides reproducible, standardised conditions so that a precise and objective analysis of all devices can be performed without the time pressure of the operating theater.

A further weakness of the present study is the idealization that is inherent to a phantom test. As was found on the analysis of PA scans (contrast ratio 1: 2), in real life, contrast ratios that are even lower than 1: 4 may be expected in many procedures.

Furthermore, the use of FWHM values for spheres of different diameters may not entirely accurately reflect the absolute detector performance. However, as the same methodology was used for each of the cameras involved, these measurements nonetheless provide an indication of the performance of each of the cameras relative to one another, which constituted the main objective of the present study.

The maximum performance of some of the systems here may even be below the lesion size tested here. Although phantoms for such tests have been described [17], we did not have these phantoms available, nor did they seem relevant for the present comparison as several of the devices used in this study were unable to detect the smaller spheres in the phantoms that were used.

A point to consider is the ease of use of the devices described here. The Portable camera system is easy to use as the camera head just needs to be positioned over the volume of interest and then acquisition can be started. Correlation of the scintigraphic image with the intraoperative findings may, however, be difficult. For this purpose, a gadolinium pointer is supplied. However, in our practical experience, the automatic localization of this pointer was inaccurate.

The practical use of declipseSPECT is more complex. Before imaging, anatomical single-use land markers need to be placed on the patient as well as on the gamma probe. Images are only available after reconstruction, thereby eliminating the possibility of real-time visualization, which is partially compensated by the display as a fusion image with the intraoperative situs that facilitates navigation [16]. In fact, in clinical practice, this method of visualization is intuitively much more comfortable and comprehensible for the user than a simple planar scintigraphic image such as that produced by, for example, the Portable camera. Practical use of the conventional probe is straightforward; a display shows the count rate for the region to which the probe is pointed. In comparison with the conventional probe, handling of the electronically collimated probe was more complex and data acquisition was more time consuming as the displayed counts are a unified derivative from the measurement of each of the five single detectors using a complex calculation rather than a directly measured radiation intensity level. The probe must be moved slowly for best results as count rates need to be acquired by five single

detectors for a certain period of time (typically about 5 s per probe position).

The clinical implications of our findings are, however, considerable. Three out of four devices failed to detect smaller lesions (0.5 ml) at technically more demanding lower contrast ratios, making them useless for the intraoperative localization of PA. One out of two devices designed for high-energy photon-mediated lesion detection failed completely to do so as soon as lower contrast ratios were introduced. Only in a condition of infinite contrast did all devices show an acceptable performance with regard to smaller lesions; therefore, all these devices can be used for SLNB without hesitation.

Under all examined conditions, freehand SPECT delivered a better image quality in comparison with the portable camera. When the contrast ratio is infinite, the image quality of freehand SPECT is similar to the results of the conventional camera. At a contrast level of 1 : 8 with spheres on the surface, freehand SPECT revealed even better results in comparison with the conventional camera. The explanation for this finding is most likely that freehand SPECT uses a 3D acquisition method whereas scintigrams acquired with the conventional camera were planar images.

As a perspective for the future, the optimal combination of properties for intraoperative imaging may be easily achieved by a fusion of the freehand SPECT methodology with the detector technology of the electronically collimated probe. This will allow for accurate intraoperative conventional gamma and PET imaging, while at the same time providing an intuitive, accurate anatomical localization technique for lesion localization.

Conclusion

All systems assessed in the present study performed adequately for the intraoperative detection of sentinel nodes with ^{99m}Tc. For technically more demanding procedures in terms of small lesion localization in a setting with low signal-to-background contrast ratios, the electronically collimated probe in our study was the only device that performed adequately, especially when ^{18}F was used.

Acknowledgements

Conflicts of interest

There are no conflicts of interest.

References

1 Vermeeren L, Van der Ent F, Sastrowijoto P, Hulsewe K. Sentinel lymph node biopsy in patients with thin melanoma: occurrence of nodal metastases and its prognostic value. *Eur J Dermatol* 2010; **20**:30–34.

2 Vermeeren L, Valdes Olmos RA, Klop WM, Balm AJ, van den Brekel MW. A portable gamma-camera for intraoperative detection of sentinel nodes in the head and neck region. *J Nucl Med* 2010; **51**:700–703.

3 Ilgan S, Ozturk E, Yildiz R, Emer O, Ayan A, Gorgulu S, *et al*. Combination of preoperative ultrasonographic mapping and radioguided occult lesion localization in patients with locally recurrent/persistent papillary thyroid carcinoma: a practical method for central compartment reoperations. *Clin Nucl Med* 2010; **35**:847–852.

4 De Nardi P, Carvello M, Canevari C, Passoni P, Staudacher C. Sentinel node biopsy in squamous-cell carcinoma of the anal canal. *Ann Surg Oncol* 2011; **18**:365–370.

5 Vermeeren L, Meinhardt W, Bex A, van der Poel HG, Vogel WV, Hoefnagel CA, *et al*. Paraaortic sentinel lymph nodes: toward optimal detection and intraoperative localization using SPECT/CT and intraoperative real-time imaging. *J Nucl Med* 2010; **51**:376–382.

6 Vermeeren L, Meinhardt W, van der Poel HG, Valdes Olmos RA. Lymphatic drainage from the treated versus untreated prostate: feasibility of sentinel node biopsy in recurrent cancer. *Eur J Nucl Med Mol Imaging* 2010; **37**:2021–2026.

7 Veronesi U, Paganelli G, Viale G, Luini A, Zurrida S, Galimberti V, *et al*. Sentinel-lymph-node biopsy as a staging procedure in breast cancer: update of a randomised controlled study. *Lancet Oncol* 2006; **7**: 983–990.

8 Britten AJ. A method to evaluate intra-operative gamma probes for sentinel lymph node localisation. *Eur J Nucl Med* 1999; **26**:76–83.

9 Ikeda Y, Takayama J, Takami H. Minimally invasive radioguided parathyroidectomy for hyperparathyroidism. *Ann Nucl Med* 2010; **24**: 233–240.

10 Meller B, Sommer K, Gerl J, von Hof K, Surowiec A, Richter E, *et al*. High energy probe for detecting lymph node metastases with ^{18}F-FDG in patients with head and neck cancer. *Nuklearmedizin* 2006; **45**: 153–159.

11 Kim WW, Kim JS, Hur SM, Kim SH, Lee SK, Choi JH, *et al*. Radioguided surgery using an intraoperative PET probe for tumor localization and verification of complete resection in differentiated thyroid cancer: a pilot study. *Surgery* 2010; **149**:416–424.

12 Freesmeyer M, Wurst C, Uberrueck T, Scholz T, Knosel T, Schulz S, *et al*. Intraoperative identification of a neuroendocrine tumour diagnosed by ^{68}Ga-DOTATOC PET but undetectable by surgical palpation or conventional imaging. *Nuklearmedizin* 2009; **48**:N50–N51.

13 Perkins AC, Britten AJ. Specification and performance of intra-operative gamma probes for sentinel node detection. *Nucl Med Commun* 1999; **20**:309–315.

14 Loening AM, Gambhir SS. AMIDE: a free software tool for multimodality medical image analysis. *Mol Imaging* 2003; **2**:131–137, *http://amide.sourcefourge.net/*.

15 Mariscal Martinez A, Sola M, de Tudela AP, Julian JF, Fraile M, Vizcaya S, *et al*. Radioguided localization of nonpalpable breast cancer lesions: randomized comparison with wire localization in patients undergoing conservative surgery and sentinel node biopsy. *Am J Roentgenol* 2009; **193**:1001–1009.

16 Wendler T, Herrmann K, Schnelzer A, Lasser T, Traub J, Kutter O, *et al*. First demonstration of 3-D lymphatic mapping in breast cancer using freehand SPECT. *Eur J Nucl Med Mol Imaging* 2010; **37**: 1452–1461.

17 Lees JE, Bassford DJ, Blackshaw PE, Perkins AC. Design and use of mini-phantoms for high resolution planar gamma cameras. *Appl Radiat Isot* 2010; **68**:2448–2451.